B physics at the LHC

Tatsuya Nakada

CERN and University of Lausanne, Switzerland

1 Introduction

Since its discovery, the b quark has brought us two big surprises. The first was the unexpectedly large lifetime. The second was the mass difference between the two mass eigenstates of the B_d meson system which is about 100 times larger than the mass difference in the neutral K meson system. From the first observation, we learned that the mixing between the second and third families is much smaller than between the first and second families. (The mixing between the first and third families is even more suppressed.) The second observation taught us that the mass of the top quark is much larger than had been anticipated at that time.

The main goal of B physics is to study the structure of quark mixing and its role in CP violation. In the Standard Model CP violation can be very naturally accommodated through the complex quark mixing matrix (Kobayashi and Maskawa 1972) defined by four parameters (Nir 2001). All current observations of CP violating phenomena in particle physics are in full agreement with the Standard Model calculations. However, there are still some reasons to speculate about CP violation generated by physics beyond the Standard Model. Firstly, the Standard Model alone cannot account for the large asymmetry between matter and antimatter observed in our universe (Shaposhnikov 1986). Secondly, various extensions to the Standard Model introduce new sources of CP violation. Since CP violation is expected in many B meson decay modes, and the Standard Model can make precise predictions for some of these decay modes, the B meson system appears to be a very attractive place to look for evidence for physics beyond the Standard Model.

In the presence of new physics, some assumptions made to extract the Cabibbo-Kobayashi-Maskawa (CKM) parameters are no longer valid. Indeed, the consistency of the CKM picture with current observations could be accidentally due to numerical cancellation between various effects from new physics. Therefore, it is essential to develop a strategy which allows the

new physics and the Standard Model contributions to be clearly disentangled. Then the CKM parameters can be determined in a model-independent way. This is important since we hope that physics at higher energy scale will one day be able to explain the family structure, by deriving the CKM parameters.

In this article, we discuss how B meson decays can be explored at the LHC in order to obtain a better understanding of the CKM picture, and to look for physics beyond the Standard Model.

2 The CKM picture

2.1 The CKM matrix

In the Standard Model, CP violation is naturally introduced by a 3×3 complex quark mixing matrix, $V_{\rm CKM}$, expressed as

$$V_{\rm CKM} = \begin{pmatrix} V_{ud} & V_{us} & V_{ub} \\ V_{cd} & V_{cs} & V_{cb} \\ V_{td} & V_{ts} & V_{tb} \end{pmatrix}.$$

The charged current of the weak interaction is then proportional to

$$\overline{U}^i_L \left(1-\gamma_5\right) \gamma_\mu V_{ij} D^j_L W^\mu$$

where U_L and D_L are the left-handed quark operators for the charge $2/3$ up-type and the charge $-1/3$ down-type quarks respectively:

$$U_L = \begin{pmatrix} u_L \\ c_L \\ t_L \end{pmatrix}, \qquad D_L = \begin{pmatrix} d_L \\ s_L \\ b_L \end{pmatrix}.$$

The matrix $V_{\rm CKM}$ is unitary, $V^\dagger V = 1$. One of the unitarity relations is:

$$V_{ud}V^*_{ub} + V_{cd}V^*_{cb} + V_{td}V^*_{tb} = 0. \tag{1}$$

This is illustrated in the complex plane in Figure 1(a). The unitarity condition can be illustrated more easily by translating $V_{cd}V^*_{cb}$ and $V_{td}V^*_{tb}$ to form a closed triangle, as shown in Figure 1(b). The three angles of the triangle, α, β and γ (also known as ϕ_2, ϕ_1 and ϕ_3 respectively) can be defined as:

$$\alpha = \tan^{-1}\left(-\frac{V_{td}V^*_{tb}}{V_{ud}V^*_{ub}}\right),\ \beta = \pi - \tan^{-1}\left(\frac{V_{td}V^*_{tb}}{V_{cd}V^*_{cb}}\right),\ \gamma = \tan^{-1}\left(-\frac{V_{ud}V^*_{ub}}{V_{cd}V^*_{cb}}\right). \tag{2}$$

It should be noted that a redefinition of the quark phases results in a rotation of the triangle in which the three angles, α, β and γ remain invariant.

Figure 1. *(a) One CKM matrix unitarity condition:* $V_{ud}V_{ub}^* + V_{cd}V_{cb}^* + V_{td}V_{tb}^* = 0$. *(b) Elements translated to form a triangle drawn in the complex plane.*

Violation of the unitarity condition given by Equation (1) is expressed in a graphical form in Figure 2(a) and (b), where the three sides given by $V_{ud}V_{ub}^*$, $V_{cd}V_{cb}^*$ and $V_{td}V_{tb}^*$ do not form a closed triangle. Note that α, β and γ defined by Equation (2) still satisfy:

$$\alpha + \beta + \gamma = \pi.$$

If one forms the closed triangle from the length of the three sides, $|V_{ud}V_{ub}^*|$, $|V_{cd}V_{cb}^*|$ and $|V_{td}V_{tb}^*|$, the three angles of this triangle, α', β' and γ' defined in Figure 2(c), are not identical to α, β and γ. Therefore, a test of unitarity can be made by comparing the angles defined by the length of the three sides, and the angles measured by CP violating effects (as explained later).

A unitary 3×3 matrix can be parameterized by four parameters. One possible choice (Particle Data Group 2000) is to use three angles, θ_{12}, θ_{23}, θ_{13} and one complex phase, δ. The standard parameterization for the CKM matrix is then given by:

$$V_{\rm CKM} = R_{23} \times R_{13} \times R_{12}$$

where

$$R_{12} = \begin{pmatrix} c_{12} & s_{12} & 0 \\ -s_{12} & c_{12} & 0 \\ 0 & 0 & 1 \end{pmatrix}, \qquad R_{23} = \begin{pmatrix} 1 & 0 & 0 \\ 0 & c_{23} & s_{23} \\ 0 & -s_{23} & c_{23} \end{pmatrix}$$

$$R_{13} = \begin{pmatrix} c_{13} & 0 & s_{13}e^{-i\,\delta} \\ 0 & 1 & 0 \\ -s_{13}e^{i\,\delta} & 0 & c_{13} \end{pmatrix}$$

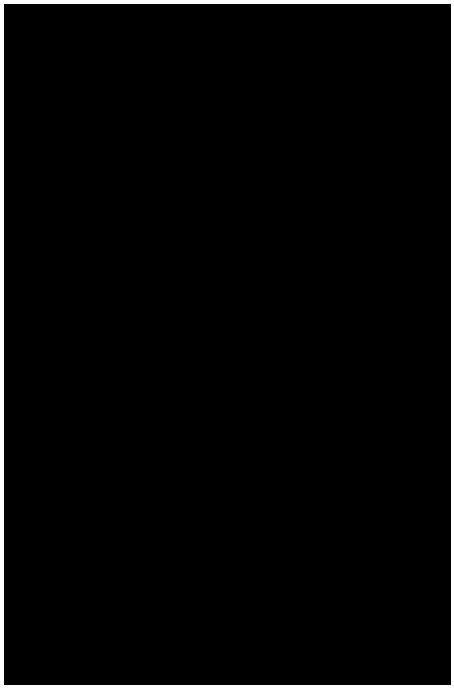

Figure 2. *(a) and (b), are similar to Figure 1, but unitarity is violated. In (c) a closed triangle is formed using the three sides.*

with $s_{ij} = \sin\theta_{ij}$ and $c_{ij} = \cos\theta_{ij}$.

A parameterization reflecting the observed pattern of the CKM matrix was proposed by Wolfenstein (Wolfenstein 1983). This introduces the parameters:

$$\lambda = s_{12}, \qquad A = \frac{s_{23}}{s_{12}^2}, \qquad \rho = \frac{s_{13}\cos\delta}{s_{12}s_{23}}, \qquad \eta = \frac{s_{13}\sin\delta}{s_{12}s_{23}},$$

and expands the matrix elements in powers of λ. Neglecting terms proportional to λ^n where $n > 5$, this gives:

$$V_{\rm CKM} \approx \begin{pmatrix} 1-\lambda^2/2 & \lambda & A\lambda^3(\rho - i\,\eta) \\ -\lambda - i\,A^2\lambda^5\eta & 1-\lambda^2/2 & A\lambda^2 \\ A\lambda^3(1-\tilde{\rho}-i\,\tilde{\eta}) & -A\lambda^2 - i\,A\lambda^4\eta & 1 \end{pmatrix} \qquad (3)$$

where $\widetilde{\rho}$ and $\widetilde{\eta}$ are given by $\widetilde{\rho} = \rho(1-\lambda^2/2)$ and $\widetilde{\eta} = \eta(1-\lambda^2/2)$. The parameter λ is known from light hadron decays to be 0.221 ± 0.002 (Particle Data Group, 2000). As seen from Equation 3, the first 2×2 sub-matrix is almost unitary:

$$V_{ud}V_{cd}^* + V_{us}V_{cs}^* = iA^2\lambda^5\eta \approx 0 \qquad V_{ud}V_{us}^* + V_{cd}V_{cs}^* = -iA^2\lambda^5\eta \approx 0$$

and

$$|V_{ud}|^2 + |V_{us}|^2 = 1 - \lambda^4/4 \approx 1 \qquad |V_{cd}|^2 + |V_{cs}|^2 = 1 - \lambda^4/4 \approx 1$$

With the parameterization given in Equation 3, the imaginary part of V_{cd} becomes negligible in the unitarity relation given by Equation (1), and the phases of the matrix elements are:

$$\arg V_{td} = -\beta, \qquad \arg V_{ub} = -\gamma,$$

$$\arg V_{ud} = \arg V_{cb} = \arg V_{tb} = 0, \qquad \arg V_{cd} = \pi.$$

V_{us} and V_{cs} are also real, but the imaginary part of V_{ts} cannot be completely ignored:

$$\arg V_{ts} = \delta\gamma + \pi$$

The angles β, γ and $\delta\gamma$ are functions of ρ, η and λ:

$$\beta = \tan^{-1}\frac{\eta}{1-\rho}, \qquad \gamma = \tan^{-1}\frac{\eta}{\rho}, \qquad \delta\gamma = \tan^{-1}\lambda^2\eta. \tag{4}$$

2.2 Extraction of the CKM parameters

From a measurement of $|V_{cb}|$, the Wolfenstein parameter A can be determined. The matrix element $|V_{cb}|$ is extracted from semileptonic (and hadronic) decays of B mesons into charmed meson final states (Stone 2001). In exclusive B meson decays, a description based on the quark tree level process $b \to c + W^-$ is obscured by soft hadronic interactions. This has to be taken into account in order to extract $|V_{cb}|$ from the data. Significant improvements in understanding these hadronic effects have been made both in theory and experiment. Further progress will come using the high statistics data samples from the BABAR and BELLE experiments (Schubert 2001).

The semileptonic decays of B mesons to final states containing only the light u and d quarks are used for the extraction of $|V_{ub}|$ (Stone 2001). They are generated by the tree level process $b \to u + W^-$. Unlike the determination of $|V_{cb}|$, hadronic decays cannot be used since sizeable contributions from the penguin processes, $b \to s$ and $b \to d$, are present in the decay amplitudes. It is much more difficult to evaluate the effects of strong interactions for $|V_{ub}|$ than for $|V_{cb}|$, and the error on the current value of $|V_{ub}|$ is totally dominated by the theoretical uncertainties. This will remain the case for some time.

While $|V_{cb}|$ and $|V_{ub}|$ are determined from decays with tree processes, $|V_{td}|$ can be accessed indirectly through loop processes such as B^0–$\overline{B}^0$ oscillations. The oscillation in the Standard Model is described by the well known box diagrams shown in Figure 3. Due to the large top quark mass and the structure of the CKM matrix, only the top quark contribution needs to be considered in the loop. Neglecting the absorptive part of the box diagrams, the oscillation amplitude for $B^0 \to \overline{B}^0$ is calculated to be (Hagelin 1981):

$$H_{21} = -\frac{G_F^2 f_{B_d}^2 B_{B_d} m_{B_d} m_W^2}{12\pi^2} \eta_{B_d} S(x_t)(V_{td}V_{tb}^*)^2 \tag{5}$$

Figure 3. *Box diagrams describing B^0–$\overline{B}^0$ oscillation.*

where G_F, m_W and m_{B_d} are the Fermi coupling constant, W boson mass and B_d mass. The function $S(x_t)$ is determined from the mass ratio, $x_t = (m_t/m_W)^2$, where m_t is the top quark mass, and the QCD correction factor, η_{B_d}, can be calculated reliably with perturbation methods. The B meson decay constant, f_{B_d}, and the bag parameter, B_{B_d}, have never been measured directly. The decay constant f_{B_d} is given by the transition matrix element between B^0 and the hadronic vacuum state. Thus it could be experimentally obtained from the branching fraction for the leptonic decay, $B^\pm \to \tau^\pm \nu_\tau$ shown in Figure 4, assuming that $|V_{ub}|$ is known. The decay constants for

Figure 4. *Diagram for the $B^+ \to \tau^+ \nu_\tau$ decay.*

$B^\pm$ and B^0 are expected to be very similar. The bag parameter takes into account the difference between the hadronic vacuum and the actual hadronic states virtually present in the B^0–$\overline{B}^0$ oscillation processes. Theoretical estimates exist with large uncertainties due to the difficulties in evaluating the effects of the non-perturbative soft hadronic interactions. The most promising theoretical approach to obtain f_{B_d} and B_{B_d} is the QCD lattice calculation discussed in these proceedings (Davies 2001).

The absorptive part in the B^0–$\overline{B}^0$ oscillation is due to c and u quarks. It is calculated to be very small compared to the dispersive part and can indeed be ignored. With this approximation, the mass difference between the two mass eigenstates, B_d^H and B_d^L, can be derived,

$$\Delta m_d \equiv m_{B_d}^H - m_{B_d}^L = 2|H_{21}|,$$

and the decay width difference between them is negligible:

$$\Delta\Gamma_d \equiv \Gamma_{B_d}^L - \Gamma_{B_d}^H \approx 0.$$

There is no CP violation in the B^0–$\overline{B}^0$ oscillations in this approximation. Note that the phase of the oscillation amplitude is given by the phase $V_{td}^2 = -2\beta$.

The mass difference Δm_d is experimentally measured as the frequency of B^0–$\overline{B}^0$ oscillations. From the known structure of the CKM matrix, we have $|V_{tb}| = 1$ with very high accuracy. Therefore, $|V_{td}|$ can be obtained from Δm_d. The error on $|V_{td}|$ is totally dominated by the theoretical uncertainties on $f_B\sqrt{B_d}$.

From the measurements of V_{ub}, V_{cb} and V_{td}, the quantities:

$$\sqrt{\widetilde{\rho}^2 + \widetilde{\eta}^2} = \frac{1}{\lambda}\frac{|V_{ub}|}{|V_{cb}|}\left(1 - \frac{\lambda^2}{2}\right) \tag{6}$$

and

$$\sqrt{(1-\widetilde{\rho})^2 + \widetilde{\eta}^2} = \frac{1}{\lambda}\frac{|V_{td}|}{|V_{cb}|} \tag{7}$$

can be drawn as circles around $(0,\ 0)$ and $(1,\ 0)$ in the $\widetilde{\rho}$–$\widetilde{\eta}$ plane respectively. There are two possible solutions where these circles intersect, but the one with $\widetilde{\eta} > 0$ is favoured from the analysis of CP violation in the K^0–$\overline{K}^0$ oscillations.

The mass difference in the B_s system, Δm_s, can be evaluated by calculating the B_s^0–$\overline{B}_s^0$ oscillation amplitude using box diagrams in a similar way to the B_d system. A measurement of Δm_s determines $|V_{ts}V_{tb}^*|^2$, which allows:

$$\sqrt{(1-\widetilde{\rho})^2 + \widetilde{\eta}^2} = \frac{1}{\lambda}\frac{|V_{td}|}{|V_{ts}|} \tag{8}$$

to be used instead of Equation (7). In the ratio:

$$\frac{1}{\lambda}\frac{|V_{td}|}{|V_{ts}|} = \frac{1}{\lambda}\frac{\sqrt{\Delta m_d}}{\sqrt{\Delta m_d}} \times \frac{\sqrt{m_{B_s}\eta_{B_s}}}{\sqrt{m_{B_d}\eta_{B_d}}} \times \frac{\sqrt{B_{B_s}}f_{B_s}}{\sqrt{B_{B_d}}f_{B_d}}\ ,$$

the assumption $|V_{tb}| = 1$ is no longer necessary. While the theoretical uncertainty in $f_B\sqrt{B}$ is quite considerable, the ratio between these quantities for the B_s and B_d mesons is theoretically much better understood. Therefore, Equation (8) will have a significantly smaller error than Equation (7). Unfortunately, only an experimental lower limit is available for Δm_s at the moment.

We now consider CP violation for decay final states which can be produced by both B^0 and $\overline{B}^0$. These can be CP eigenstates such as $J/\psi\, K_S$ or non-CP eigenstates such as $D^{*+}\pi^-$ and its CP-conjugate state $D^{*-}\pi^+$. If CP violation is present neither in the oscillation nor the decay amplitudes, it is well known that the only signature of CP violation that can appear is through phases:

$$\sin(\phi_0 + \phi_f)\sin(\Delta m_d t)$$

in the time-dependent decay rates of initial B^0 and $\overline{B}^0$, where ϕ_0 is the phase of the B^0–$\overline{B}^0$ oscillation amplitude, and ϕ_f is the phase of the ratio of the instantaneous decay amplitudes of B^0 and $\overline{B}^0$ into the particular final state.

For the $J/\psi\, K_S$ final state, the $b \to c + W^-$tree process dominates, but there can also be a $b \to s$ penguin process (Figure 5). The phase of the tree process is given by V_{cb}, and is 0 in the Wolfenstein approximation. The penguin process is described by a virtual top quark loop with CKM matrix elements, $V_{tb}V_{ts}^*$, which has only a small phase $-\delta\gamma$. Therefore, $\phi_f = 0$, with a theoretical uncertainty less than a few percent.

Figure 5. *Quark diagrams for the $\overline{B}^0 \to J/\psi\, K_S$ decay.*

The final state $D^{*+}\pi^-$ can be generated by the tree process $b \to c + W^-$, followed by $W^- \to \overline{u}d$ for the $\overline{B}^0$ decay or the doubly Cabibbo-suppressed tree process $\overline{b} \to \overline{u} + W^+$ followed by $W^+ \to c\overline{d}$ for the B^0 decay, as seen from Figure 6. From the relevant CKM matrix elements, it follows that $\phi_f = \gamma$. Note that only the tree processes contribute.

The phase of the oscillation amplitude is given by $\phi_0 = 2\beta$ as discussed before. Therefore the CP violation signatures in B^0 and $\overline{B}^0$ decays are

$$\sin(2\beta)\sin(\Delta m_d t) \qquad \text{for} \quad J/\psi\, K_S$$

and

$$\sin(2\beta+\gamma)\sin(\Delta m_d t) \qquad \text{for} \quad D^{*+}\pi^- \text{ and } D^{*-}\pi^+.$$

For the $\sin(2\beta)$ measurement from $J/\psi\, K_S$, the average of the recent results from BABAR and BELLE gives (Schubert 2001):

$$\sin 2\beta = 0.79 \pm 0.17$$

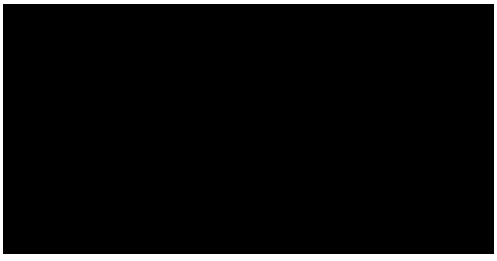

Figure 6. *Quark diagrams for the B^0 and $\overline{B}^0 \to D^{*+}\pi^-$ decays.*

where the error is scaled following the recipe of the Particle Data Group. It is unlikely that any definitive measurement of $\sin(2\beta+\gamma)$, using $B \to D^{(*\pm)}\pi^{(\mp)}$, will be done by the current generation of experiments.

Analogous decays for the B_s^0 meson system are $J/\psi\,\phi$ and $J/\psi\,\eta$, which have $\phi_f = 0$, and $D_s^+ K^-$ which has $\phi_f = \gamma$. Since the B_s^0–$\overline{B}_s^0$ oscillation phase is $-2\delta\gamma$ as discussed before, the CP violation signatures would be:

$$\sin(-2\delta\gamma)\sin(\Delta m_s t) \quad \text{for} \quad J/\psi\,\phi \text{ (or } J/\psi\,\eta)$$

and

$$\sin(-2\delta\gamma+\gamma)\sin(\Delta m_s t) \quad \text{for} \quad D_s^+ K^- \text{ and } D_s^- K^+.$$

No definitive measurements on these quantities will be available from the current generation of experiments.

In Figure 7, we summarise the region of $\widetilde{\rho}$ and $\widetilde{\eta}$ allowed by the current data on $|V_{ub}|/(\lambda|V_{cb}|)$, Δm_d, and $\sin(2\beta)$, as well as the one-sided constraint on $\Delta m_d/\Delta m_s$ from the lower limit on Δm_s. All the data are interpreted within the framework of the Standard Model, so the constraints may be modified by new physics as discussed earlier. There is a common overlapping region indicating that the data are consistent with the CKM picture, and no sign of new physics is visible within the errors. Note that the $\sin(2\beta)$ measurement gives two allowed regions in the $\widetilde{\rho}$–$\widetilde{\eta}$ plane defined in Figure 7, and only the one consistent with the other constraints is drawn.

Figure 7. *Allowed region in the $\widetilde{\rho}$–$\widetilde{\eta}$ plane from $|V_{ub}|/|V_{cb}|$, Δm_d, and $\sin(2\beta)$ measurements, and from the upper limit on Δm_s.*

3 Possible CKM picture in 2006

Let us now speculate about the CKM landscape in 2006. Due to progress in theoretical understanding of the hadronic effect, strongly helped by the large statistics and high quality data from BABAR and BELLE, $|V_{ub}/V_{cb}|$ might become known with a relative error of $\pm 10\%$. Once Δm_s is measured by CDF, $|V_{td}|/(\lambda|V_{ts}|)$ will become known with a relative error of $\pm 7\%$. From CP violation in B^0 and $\overline{B}^0$ decays to $J/\psi\,K_S$, the combined results from BABAR, BELLE, CDF and D0 might yield a result of $\sin(2\beta)$ with an error as small as 0.03, which is still statistically limited. Estimating the progress in other CP violation channels is more difficult since they have various theoretical uncertainties, and future improvements are difficult to evaluate. Assuming

that the currently preferred values of ρ and η remain unchanged, the situation expected in 2006 is illustrated in Figure 8.

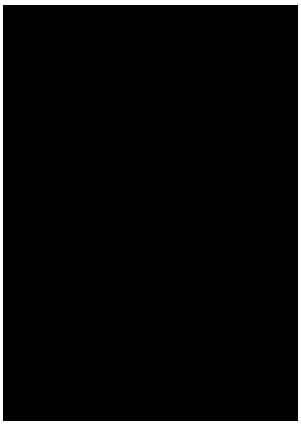

Figure 8. *Possible situation of the allowed region in the $\widetilde{\rho}$–$\widetilde{\eta}$ plane in 2006*

4 Presence of New Physics

Once we allow the presence of physics beyond the Standard Model, the determination of the CKM matrix elements becomes much more complicated. Most of the extensions of the Standard Model introduce new heavy particles. The contributions of these particles to the tree processes should be negligible, but for B^0–$\overline{B}^0$ and B_s^0–$\overline{B}_s^0$ oscillations, their contribution to the box processes could be sizeable. New heavy particles could also appear in the penguin processes, but the effects should be smaller than in the box processes, due to the different dependence on the masses of the particles appearing in the loops.

In the presence of new physics, the phases for the oscillation amplitudes are modified:

$$\phi_0^d = 2\beta + \phi_{\rm NP}^d$$

and

$$\phi_0^s = -2\delta\gamma + \phi_{\rm NP}^s$$

where $\phi_{\rm NP}^d$ and $\phi_{\rm NP}^s$ are new phases.

The new physics has very little effect on the decay amplitude if this is generated by tree processes. Therefore, we assume that the phases of the amplitudes for decay modes such as $B^0 \to J/\psi\, K_S$, $B^0 \to D^{*+}\pi^-$, $B_s^0 \to J/\psi\,\phi$ and $B_s^0 \to D_s^+ K^-$ remain unchanged. For the CP violation signatures in B^0 and $\overline{B}^0$ decays, we would then have

$$\sin(2\beta + \phi_{\rm NP}^d)\sin\Delta m_d t \qquad \text{for} \quad J/\psi\, K_S \tag{9}$$

and

$$\sin(2\beta + \phi^d_{\rm NP} + \gamma) \sin \Delta m_d t \qquad \text{for} \quad D^{*+}\pi^- \text{ and } D^{*-}\pi^+.$$

The value of β is modified, but it is possible to use both measurements to extract the angle, γ, in a theoretically clean way, even if new physics is present.

Similarly for the B^0_s system:

$$\sin(-2\delta\gamma + \phi^s_{\rm NP}) \sin(\Delta m_s t) \qquad \text{for} \quad J/\psi\,\phi \text{ (or } J/\psi\,\eta) \tag{10}$$

and

$$\sin(-2\delta\gamma + \phi^s_{\rm NP} + \gamma) \sin(\Delta m_s t) \qquad \text{for} \quad D^+_s K^- \text{ and } D^-_s K^+.$$

the value of $\delta\gamma$ is modified, but γ can be cleanly extracted by combining the two CP violation measurements.

Once γ is determined, ρ and η are given by:

$$\rho = \frac{1}{\lambda}\frac{|V_{ub}|}{|V_{cb}|}\cos\gamma, \qquad \eta = \frac{1}{\lambda}\frac{|V_{ub}|}{|V_{cb}|}\sin\gamma\ ,$$

and the unmodified values of β and $\delta\gamma$ can be obtained from Equation (4). Hence all the parameters of the CKM matrix can be completely determined even if new physics exists. The contributions from new physics are then determined from Equations (9) and (10).

The allowed region in $\widetilde{\rho}$–$\widetilde{\eta}$ plane from the CP asymmetry measurement with B^0 and $\overline{B}^0 \to J/\psi\, K_S$ decays is no longer valid. What is measured from the asymmetry is not β, but $\beta + \phi^d_{\rm NP}/2$. Similarly, the region given by the $\Delta m_d/\Delta m_s$ measurements is no longer valid since there could be sizeable contributions to both the Δm from new physics. The only valid region in Figure 8 is that from the $|V_{ub}|/(\lambda|V_{cb}|)$ measurement, and the apparent consistency seen in Figure 8 could be accidental. Once γ is measured in the theoretically clean way explained above,

In the discussion above, we have made an assumption that new physics does not contribute to the decay amplitude. This may not be strictly true for the $B^0 \to J/\psi\, K_S$ and $B^0_s \to J/\psi\,\phi$ decays, since these decays receive a small contribution from the $b \to s$ penguin process. Whether new physics can appear in the penguin process can be examined by studying CP violation in B^0 and $\overline{B}^0$ decays into ϕK_S. In the Standard Model the decay amplitude is dominated by a loop with the virtual top quark, so the phase is given by V_{ts}, and the CP violation signature is:

$$\sin(2\beta + \phi^d_{\rm NP} - 2\delta\gamma + \phi^{\rm P}_{\rm NP}) \sin(\Delta m_d t)\ , \tag{11}$$

where $\phi^{\rm P}_{\rm NP}$ is the additional phase introduced in the $b \to s$ penguin process by new physics. By comparing Equations (9) and (11), it is possible to determine whether new physics contributes significantly to penguin processes.

New physics contributions to the $b \to d$ penguin processes can be studied from CP violation in B^0 and $\overline{B}^0$ decaying into $K^{*0}\overline{K}^{*0}$ or $\phi\pi^0$ where only

the $b \to d$ penguin process contributes in the Standard Model. Independent studies of $b \to s$ and $b \to d$ penguins can be made with the B_s system.

In conclusion, a theoretically clean and model-independent determination of the parameters of the CKM matrix is possible, even if there are new physics contributions to CP violation observables. Once the CKM parameters are determined in a model independent way, the possible existence of new physics can be cleanly established.

5 *B* experiments at the LHC

5.1 General considerations

The goal of B physics in the LHC era (Ahmadov et al, 2000) is to determine the CKM parameters in a model-independent way and to isolate the effect of new physics so that its characteristics can be identified. This calls for an high statistics experiment capable of studying CP violation with both B_d^0 and B_s^0 systems decaying into various hadronic final states.

The production cross section for $b\bar{b}$ quark pairs at the LHC energy is estimated to be approximately 500μb, which is far larger than at existing machines. The fraction of events with b quarks, $\sigma_{b\bar{b}}/\sigma_{\rm inelastic}$, is about 6×10^{-3}, which is similar to the fraction of charm events in present fixed-target charm experiments. Thus, the LHC appears to be a very promising place to perform high precision CP violation measurements in B meson decays. At the LHC, B_s, $\overline{B}_s$, $B_c^{\pm}$ and b-baryons are abundantly produced, in addition to $B^{\pm}$, B^0 and $\overline{B}^0$.

In order to exploit the full potential of the LHC, the following capabilities are needed.

1. A trigger sensitive to both leptonic and hadronic final states.
2. A particle identification system capable of identifying p, K, π, μ and e within the required momentum range.
3. A vertex detector able to reconstruct primary and B vertices very precisely.
4. A tracking system with good momentum resolution.
5. An electromagnetic calorimeter capable of reconstructing π^0 decays.

5.2 The ATLAS and CMS experiments

ATLAS (Armstrong 1994) and CMS (Bayatian 1994) are two general purpose collider detectors designed to perform high p_T physics at the LHC, including studies of the top quark, detection of the Higgs boson, and searches for supersymmetric particles. They detect $b\bar{b}$ quark pairs in the central region of the pp

interactions. As already demonstrated by CDF, such general purpose collider experiments can cleanly reconstruct B meson final states containing lepton pairs, such as $J/\psi\, K_S$, $J/\psi\phi$ and $\ell^+\ell^-$. Both ATLAS and CMS have excellent muon and electron detection capabilities, and a good vertex resolution, allowing them to collect a high statistics sample of such decays. However, their first level trigger on a high p_T lepton is not sensitive to purely hadronic final states. Hadronic decay modes can only be triggered by a semileptonic decay of the other b quark, which has a low efficiency due to the relatively small branching fraction for the semileptonic decay. The two experiments also have no $p/K/\pi$ separation capability in the relevant momentum range, although the energy loss, dE/dx, can be used for particle identification at low momenta. In particular they cannot separate kaons from pions in the high momentum region relevant for two-body decay modes of B mesons such as $\pi^+\pi^-$ and D_sK.

For these reasons, ATLAS and CMS will not be able to study CP violation with all the final states necessary to perform model-independent analysis.

5.3 The LHCb experiment

The LHCb experiment is a single arm forward spectrometer, which covers the region of pp collisions which is not looked at by the two general purpose detectors. The LHCb detector (Amato 1998) is designed to have a trigger that is equally efficient for leptons and hadrons. It will be able to exploit the full b physics potential of the LHC at a much lower luminosity ($2 \times 10^{32}\mathrm{cm}^{-2}\mathrm{s}^{-1}$) than the nominal luminosity ($10^{34}\mathrm{cm}^{-2}\mathrm{s}^{-1}$), and will therefore be able to perform its full physics programme from the beginning of LHC operation.

The detector layout is shown in Figure 9. It resembles a typical fixed target spectrometer. A vertex detector is placed in "Roman pots" around the interaction region. It is followed by a tracking system, RICH counters with aerogel and gas radiators, a large-gap dipole magnet, a calorimeter system, and a muon system. An existing LEP experimental area will be reused to install the detector. The interaction point is shifted by 11m from the centre of the experimental hall, in order to accommodate the detector elements without extra excavation.

The choice of a single arm detector geometry is based on the fact that both the b- and $\bar{b}$-hadrons are predominantly produced in the same forward (or backward) cone at high energies. The polar angle is defined with respect to the beam axis in the pp center-of-mass system. Detecting both b- and $\bar{b}$-hadron at the same time is essential for the flavour tag.

Further advantages of the forward geometry are:

- The b-hadrons produced are faster than those in the central region. Their average momentum is about 80GeV/c, corresponding to a mean decay length of $\sim$7mm. Therefore, a good decay time resolution can be obtained for reconstructed B-mesons.

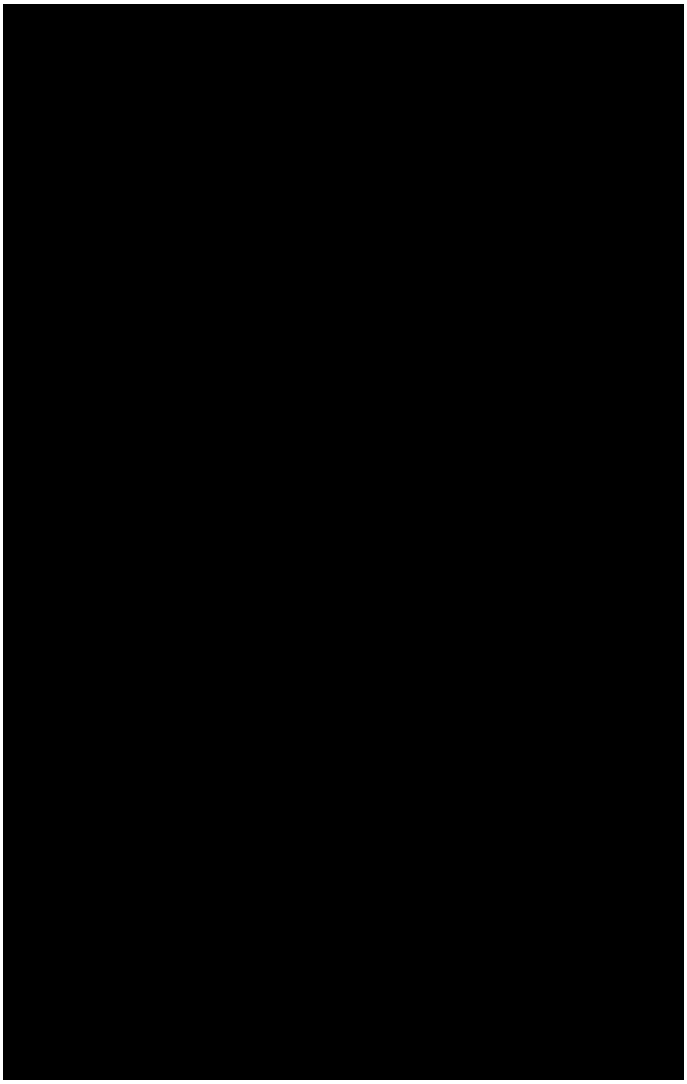

Figure 9. *The LHCb spectrometer placed in the LHC Intersection-8 experimental area.*

- The spectrometer can be built in an open geometry with an interaction region which is not surrounded by all the detector elements. This allows the vertex detector system to be built with sensors which can be extracted away from the beam during the injection. During data taking, the sensors are positioned closer to the beam in order to achieve a good vertex resolution.

- In the forward region, momenta are mainly carried by the longitudinal components. Therefore, the threshold value for the p_t trigger can be set low for electrons, muons and hadrons without being constrained by the detector requirements. This makes the p_t trigger more efficient than in the central region.

- The momentum range required for particle identification is well matched to the Ring Imaging Cherenkov Counters, and the required size for the counters remains affordable.

- The open geometry allows easy installation, maintenance and possible upgrades.

5.4 The LHCb detector

Beam pipe

A large vacuum tank with a length of 1.7m and a diameter of 1m is placed around the interaction point to accommodate the vertex detector system with its retraction mechanics. It has a 2mm Al forward exit window over the full detector acceptance. This part is followed by two conical beam pipe sections; the first part is 1.4m long with a 25mrad opening angle, and the second part is 16m long with a 10mrad opening angle. Except for bellows, flanges and the last 6.3m of the 10mrad cone, the beam pipe is made from Al-Be alloy in order to reduce the radiation length. This is essential to minimize the occupancies of the tracking and RICH systems, and to improve the detection efficiency for photons and electrons.

Magnet

A dipole magnet with an Al conductor provides a field integral of 4 Tm. The polarity of the field can be changed to reduce systematic errors in the CP-violation measurements that could result from a left-right asymmetry of the detector. The two pole faces form a wedge shape following the spectrometer acceptance, in order to reduce the power consumption.

Vertex locator (VELO)

A total of 27 stations of silicon microstrip detectors are placed perpendicular to the beam of which 25 stations are used as a vertex detector system. The remaining two stations are used for detecting bunch crossings with more than one pp interaction as a part of the Level-0 trigger (pile-up veto counters). All the stations are split into two halves, covering left and right 180° sections.

Each vertex detector station consists of two sensor planes with different strip layouts, one for r and the other for ϕ measurements. The pile-up veto counters have only r measurement sensors.

The closest distance between the active silicon area and the beam is 8mm. In order to cope with the high radiation dose expected so close to the beam, it is planned to use n-on-n silicon sensors. The silicon detectors are placed in Roman pots surrounded by 250μm thick aluminium foil, which acts as a shield against RF pickup from the circulating beam bunches. To avoid mechanical collapse, a secondary vacuum is maintained inside the Roman pots. During injection and acceleration, the Roman pot system will be moved away from the beam to avoid interference with the machine operation and accidental irradiation of the detectors.

For each bunch crossing, i.e. every 25ns, the signals are read-out and stored in analogue pipeline buffers.

Tracking system

Because of the high particle density close to the beam pipe, the LHCb tracking detector is split into inner and outer systems. The boundary between the two is chosen so that the occupancy of the outer tracker does not exceed 15%.

The outer tracking system uses drift chambers based on a straw cell structure. The straws are made by winding 5mm diameter carbon-loaded Kapton foil around a central anode wire. The drift-time is sampled over 50ns, i.e.every two bunch crossings.

The inner tracking system is made from single sided p-on-n Si strip detectors with a strip pitch of $\sim$200μm. Since the sensitive regions of the Si sensor are several centimetres away from the beam the problem of radiation damage is less severe than for the VELO detectors.

The RICH detectors

The LHCb detector has two Ring Imaging Čerenkov (RICH) systems, with three different radiators, in order to cover the required momentum range, 1–100GeV/c. The first RICH uses aerogel and C_4F_{10} gas as radiators. The second RICH, uses CF_4 gas as a radiator. It is placed after the magnet, and is responsible for identifying high momentum particles. In both RICHs the Cherenkov light is reflected by mirrors and detected with planes of Hybrid Photon Detectors (HPD's) placed outside the spectrometer acceptance.

Calorimeters

The calorimeter system consists of a preshower detector followed by electromagnetic and hadronic calorimeters. It also serves as the initial part of the muon filter system. The cells of the preshower detector are made from two scintillator plates sandwiching 14mm-thick lead plates. The cell size of the preshower detector is matched to the module size of the electromagnetic calorimeter. For the electromagnetic part a Shashlik calorimeter is used since a modest energy resolution is required. The hadron calorimeter is based on a scintillating tile design similar to that used in the ATLAS experiment.

Muon detectors

For the muon stations Resistive Plate Chambers are used in the region where the charged particle rate is below 1kHz/cm^2. For the region with a charged particle rate from 1kHz/cm^2 to 100kHz/cm^2, Multi Wire Proportional Chambers (MWPC's) are used. For the small region of the first muon station closed to the beam pipe, where the charged particle rate exceeds 100kHz/cm^2, triple-GEM chambers or MWPC's with asymmetric gas gaps are being considered.

Trigger

The LHCb trigger is divided into four decision levels. The Level-0 decision is based on high-p_T hadrons, electrons or photons found in the calorimeter system, or muons found in the muon system. Information on these candidates are sent to the Level-0 Decision Unit. The number of primary vertex candidates is determined using the pile-up veto counters in the Vertex Locator and also sent to the Level-0 Decision Unit. Based on all the information, the Level-0 Decision Unit makes an overall Level-0 decision. Events with multiple pp interactions are discarded, since rejection of background is more difficult in those events. The Level-0 trigger provides a modest reduction of minimum bias events by a factor of $\sim$10.

In the Level-1 trigger, data from the vertex detector is used to select events with multiple vertices. In addition, the high-p_T candidates used in Level-0 can be combined with the tracks having large impact parameter in the Vertex Locator. This provides a further reduction of $\sim$25 for minimum bias events. After a positive decision of the Level-1 trigger, all the data is read out into an event buffer.

At Level-2, a further enhancement of events with b-hadrons can be achieved by combining different detector components, e.g. by adding momentum information from the main tracking system to the impact parameter calculation with the Vertex Locator. At Level-3, a further decision is made after fully reconstructing the b decays.

The LHCb trigger system is designed to cope with the rather small value for $\sigma_{b\bar{b}}/\sigma_{\text{inelastic}}$ of $\sim 6 \times 10^{-3}$ at the LHC energies, while still maintaining a high efficiency for events with b hadrons. The strategy is to spread the suppression factors evenly and not to rely on any single trigger selection, in particular at early levels where available information from the detector is limited. This is reflected in the modest suppression factors of 10 and 25 for the ordinary pp interaction events at Level-0 and Level-1, respectively. Simulations of the trigger performance can be relied upon for such a modest suppression. By not heavily relaying on a particular selection criterion, the trigger system is flexible and can be readjusted to the actual running conditions of the experiment.

5.5 Performance of the LHCb detector

The benefit of having particle identification and good invariant mass resolution can be demonstrated by reconstructing $B_s \to D_s^+ K^-$ decays. The main background to this decay mode comes from the $B_s \to D_s^+ \pi^-$ decays which are used to study B_s–$\overline{B}_s$ oscillations. Compared to this decay mode, the branching fraction of $B_s \to D_s^+ K^-$ is suppressed by a factor of $1/\lambda^2 \approx 20$. The two decay modes have an identical decay topology, and can only be distinguished by invariant mass and particle identification. It should be noted that the momenta of the K^- and π^- from these decay modes are large since they are two-body decays.

Figure 10. *The LHCb simulation results for the reconstructed invariant mass distributions for $D_s^+ K^-$ combinations without and with particle identification using RICH.*

Figure 10 shows the reconstructed invariant mass distributions expected with the LHCb detector for $D_s^+ K^-$ combinations without and with particle identification using RICH. The combination of the good mass resolution, $\sigma = 11\text{MeV}/c^2$, and RICH particle identification, mean that the background from $B_s \to D_s^+ \pi^-$ decays can be almost completely removed in the reconstructed $D_s^+ K^-$ sample. It should be noted that no CP violation effect is expected in the background decay mode. The decay time resolution for these decays is found to be 40fs.

Decay Mode	Level-0 high-p_T			Level-0
	muon	electron	hadron	all combined
$B^0 \to J/\psi(e^+e^-)K_S$	0.17	0.63	0.17	0.72
$B^0 \to J/\psi(\mu^+\mu^-)K_S$	0.87	0.06	0.16	0.88
$B_s \to D_s^+K^-$	0.15	0.09	0.45	0.54
$B^0 \to \pi^+\pi^-$	0.14	0.08	0.70	0.76

Table 1. *Level-0 trigger efficiencies for reconstructed and flavour tagged final states.*

With the particle identification capability, an efficient flavour tag can be obtained using the charged kaons from the b hadron decays. No lepton is required in the analysis for flavour tagging. Therefore, the Level-0 high p_T hadron trigger increases significantly the statistics of the flavour-tagged sample of pure hadronic B decay final states, compared to using the high p_T lepton trigger alone. Table 1 summarises the Level-0 trigger efficiencies for various decay modes. Efficiencies are calculated for those events where the initial flavour is identified and the final state is fully reconstructed with all the cuts applied to remove background. While $J/\psi K_S$ final states are mainly triggered by the muon and electron high-p_T triggers, the hadron high-p_T trigger is essential for the other final states.

The table also indicates that the Level-0 trigger efficiencies are very high for the events that are useful in the analysis. As a result, the LHCb experiment will run with a luminosity of $2 \times 10^{32}\text{cm}^{-2}\text{s}^{-1}$ and still collect 2.4k reconstructed and flavour-tagged B_s and $\overline{B}_s$ decays into $D_s^+K^-$ and $D_s^-K^+$ in one year. With these statistics, γ can be measured with an accuracy of $\sim 10^\circ$. By combining the result from the decays of B^0 and $\overline{B}^0$ into $D^{*+}\pi^-$ and $D^{*-}\pi^+$, γ will be measured with a precision of better than 7° with one year of data taking.

At a low luminosity, the bunch interactions are dominated by events with only one pp collision. The running luminosity will be locally tuned at the LHCb intersection such that the experiment can run with this optimal luminosity while the other LHC experiments run at the design luminosity. It must be noted that running at lower luminosities has the additional benefit that the radiation damage to the detector is reduced.

6 Conclusions

CP violation outside the neutral kaon system has been observed for the first time by BABAR and BELLE experiments, in the decays of B^0 and $\overline{B}^0$ into the $J/\psi\, K_S$ final state. Current analysis shows that all the measurements

related to b hadron decays are consistent with the CKM picture, including CP violation. Although BABAR, BELLE, CDF and D0 will further enhance these studies in the near future, a new generation of experiments at the LHC is needed in order to examine the CKM picture in a model-independent way. It should be noted that a dedicated experiment at the Tevatron (Kulyavtsev 2000) would have a similar performance. LHCb is a dedicated detector for B physics at the LHC with particle identification capability and a trigger sensitive to both leptonic and hadronic final states, which should be able to study CP violation in both B^0 and B_s^0 meson systems in many decay modes. Some of those decay modes are essential to determine the CKM parameter in a theoretically clean and model-independent way. This will allow the effect of possible new physics to be identified unambiguously.

Acknowledgments

I thank the organizers of the school for their hospitality and creating a stimulating environment. R. Forty and O. Schneider are deeply acknowledged for many useful comments and suggestions on this manuscript.

References

Ahmadov, A. et al (2000) *Proceedings of the Workshop on Standard Model Physics (and more) at the LHC*, CERN 2000-04 .

Amato, S. (1998), *LHCb Technical Proposal*, CERN/LHCC/98-4.

Armstrong, W. W. (1994), *ATLAS Technical Proposal*, CERN/LHCC/94-43.

Bayatian, G. L. (1994), *CMS Technical Proposal*, CERN/LHCC/94-38.

Davies, C. (2001) *This volume.*

Groom, D.E. et al. [Particle Data Group] (2000), *The European Physical Journal* **C15**, 1

Hagelin, J. S. (1981), *Nucl. Phys.* **B193**, 123. For more details, see Buras, A. J, (1999),
Proceedings of 14th Lake Louise Winter Institute (Singapore: World Scientific).

Kobayashi, M. and Maskawa, K. (1972), *Prog. Theor. Phys.* **49**, 282.

Kulyavtsev, A. (2000), *BTeV Proposal*, BTeV-doc-66-v1 .

Nir, Y. (2001) *This volume.*

Shaposhnikov, M.E. (1986), *JETP Lett.* **44**, 364.

Schubert, K.R. (2001), *This volume.*

Stone, S. (2001), *This volume.*

Wolfenstein, L. (1983), *Phys. Rev. Lett.* **51**, 1945.